Cell, Vol. 95, 891–902, December 23, 1998, Copyright ©1998 by Cell Press

A Critical Role for DNA End-Joining Proteins in Both Lymphogenesis and Neurogenesis

Yijie Gao,[1] Yi Sun,[2] Karen M. Frank,[1] Pieter Dikkes,[2] Yuko Fujiwara,[3] Katherine J. Seidl,[1] JoAnn M. Sekiguchi,[1] Gary A. Rathbun,[1] Wojciech Swat,[1] Jiyang Wang,[4,8] Roderick T. Bronson,[5] Barbara A. Malynn,[1] Margaret Bryans,[6] Chengming Zhu,[1] Jayanta Chaudhuri,[1] Laurie Davidson,[1] Roger Ferrini,[1] Thomas Stamato,[6] Stuart H. Orkin,[3] Michael E. Greenberg,[2] and Frederick W. Alt[1,7]

[1]Howard Hughes Medical Institute
The Children's Hospital
The Center for Blood Research and
Department of Genetics
Harvard University Medical School
Boston, Massachusetts 02115

[2]Department of Neurology
Children's Hospital
Boston, Massachusetts 02115

[3]Howard Hughes Medical Institute
Department of Pediatrics
The Children's Hospital
Boston, Massachusetts 02115

[4]Medical Institute of Bioregulation
Kyushu University
Maidashi 3-1-1
Higashi-ku, Fukuoka 812
Japan

[5]Department of Pathology
Tufts University Schools of Medicine
and Veterinary Medicine
Boston, Massachusetts 02111

[6]Lankenau Medical Research Center
100 Lancaster Avenue
Wynnewood, Pennsylvania 19096

Summary

***XRCC4* was identified via a complementation cloning method that employed an ionizing radiation (IR)-sensitive hamster cell line. By gene-targeted mutation, we show that XRCC4 deficiency in primary murine cells causes growth defects, premature senescence, IR sensitivity, and inability to support V(D)J recombination. In mice, XRCC4 deficiency causes late embryonic lethality accompanied by defective lymphogenesis and defective neurogenesis manifested by extensive apoptotic death of newly generated postmitotic neuronal cells. We find similar neuronal developmental defects in embryos that lack DNA ligase IV, an XRCC4-associated protein. Our findings demonstrate that differentiating lymphocytes and neurons strictly require the XRCC4 and DNA ligase IV end-joining proteins and point to the general stage of neuronal development in which these proteins are necessary.**

[7]To whom correspondence should be addressed (e-mail: alt@rascal.med.harvard.edu).

[8]Present address: Division of Pathology, Chiba Cancer Center Research Institute, 666-2 Nitona-cho, chao-ku, Chiba 260-8717, Japan.

Introduction

Efficient repair of DNA double-strand breaks (DSBs) is crucial for maintenance of genomic integrity. If unrepaired, such lesions may be cell lethal (Chu, 1997). DSBs can be induced in all mammalian cell types during oxidative metabolism and by genotoxic agents such as ionizing radiation (IR). DSBs are also created in germ cells during meiotic recombination, in B and T lymphocytes during V(D)J recombination (Chu, 1997), and in B lymphocytes, possibly, during class switch recombination (CSR) (Wuerffel et al., 1997). In mammalian cells, repair of DSBs (DSBR) is achieved by both nonhomologous end joining (NHEJ) and homologous recombination repair pathways. Defects in the NHEJ pathway lead to severe consequences in cells, ranging from increased IR sensitivity to premature senescence (Smider and Chu, 1997). The importance of the NHEJ pathway is particularly evident in lymphocytes, as mutations that inactivate its components cause premature death of cells attempting to undergo V(D)J recombination and CSR (Chang et al., 1995; Casellas et al., 1998; Manis et al., 1998).

Much recent knowledge of the functions of NHEJ components in DSBR derives from V(D)J recombination studies. The site-specific V(D)J recombination reaction is targeted by conserved recombination signal sequences (RS) that flank each immunoglobulin (Ig) or T cell receptor (TCR) germline V, D, and J coding segment. The lymphocyte-specific RAG1 and RAG2 proteins initiate the reaction by introducing DSBs between coding segments and flanking RS, resulting in blunt 5′-phosphorylated RS ends and hairpin coding ends (Gellert, 1997). Subsequently, V(D)J recombination becomes a DSBR reaction that employs several generally expressed proteins, initially identified based on studies of IR-sensitive cell lines and mice homozygous for the *scid* mutation (SCID mice) (Smider and Chu, 1997). These "DSBR/V(D)J factors" include Ku80 and DNA-PKcs, two of the three subunits of the DNA-dependent protein kinase (DNA-PK) holoenzyme, as well as the XRCC4 protein (Li et al., 1995). The roles of two additional DSBR/V(D)J factors, Ku70 and ligase IV, implicated based on association with Ku80 and XRCC4, respectively (Errami et al., 1996; Critchlow et al., 1997; Grawunder et al., 1997), were demonstrated by gene-targeted mutation studies (Gu et al., 1997b; Frank et al., 1998; Grawunder et al., 1998).

The DNA-PK holoenzyme is comprised of the catalytic subunit (DNA-PKcs) and Ku, a heterodimer of Ku70 and Ku80; Ku binds to DSBs leading to activation of DNA-PKcs. Ku70- and Ku80-deficient mice are viable, although small and immunodeficient; in addition, their cells have defects in DNA end joining, which manifest as IR sensitivity, growth defects, premature senescence, and inability to rejoin both coding and RS ends during V(D)J recombination (Nussenzweig et al., 1996;

Zhu et al., 1996; Gu et al., 1997a, 1997b; Ouyang et al., 1997). In contrast, DNA-PKcs-deficient mice generated by gene-targeted mutation, like classical SCID mice, were of normal size, had variable cellular IR sensitivity, and were immunodeficient due to defects in V(D)J coding, but not RS, end joining (Gao et al., 1998; Taccioli et al., 1998). The difference in the Ku-deficient versus DNA-PKcs-deficient phenotypes implied DNA-PK-independent Ku functions (Gao et al., 1998).

We previously employed complementation cloning to isolate a cDNA sequence, termed *XRCC4*, that rescued the V(D)J recombination defects of the IR-sensitive XR-1 cell line (Li et al., 1995). The *XRCC4* gene encodes a ubiquitously expressed nuclear protein of 334 amino acids that homodimerizes (Li et al., 1995; Mizuta et al., 1997). Although the XRCC4 amino acid sequence revealed no clues as to its function, the finding that XRCC4 associates with ligase IV suggested that XRCC4 may recruit and/or activate ligase IV to complete the DSBR and V(D)J recombination end-joining reaction (Critchlow et al., 1997; Grawunder et al., 1997). In support of this notion, studies of *S. cerevisiae* mutants implicated the yeast DNA ligase IV homolog as epistatic to the yeast homologs of Ku and XRCC4 in a NHEJ pathway (Schar et al., 1997; Teo and Jackson, 1997; Wilson et al., 1997; Herrmann et al., 1998).

To characterize the in vivo role of XRCC4, we now have inactivated the *XRCC4* gene in mice via gene-targeted mutation. We show that XRCC4 deficiency leads to many cellular and lymphocyte developmental defects also found in the context of Ku and ligase IV deficiency, suggesting that they result from an impaired DNA end-joining pathway that involves Ku, ligase IV, and XRCC4. In contrast to Ku deficiency, we find that XRCC4 deficiency leads to embryonic lethality in conjunction with massive apoptotic death of newly generated, postmitotic neuronal cells throughout the developing nervous system. As we also find this neuronal death phenotype in ligase IV–deficient mice, it too may result from impaired DNA end joining.

Results

Targeted Inactivation of the *XRCC4* Gene

We have characterized the mouse *XRCC4* gene and found it to span more than 60 kb, with most exons spaced at least 10 kb apart. To inactivate this gene, we replaced exon 3, which encodes part of the XRCC4 functional core region (Mizuta et al., 1997), with a *lox*P flanked neomycin resistance gene (neo^r) in the antisense transcriptional orientation. Any potential transcript from the targeted allele that was spliced from exon 2 to either exon 4 or 5 would harbor a frameshift mutation, resulting in deletion of at least 50% of the encoded polypeptide (Figure 1A). We isolated multiple clones that had the replacement mutation on one allele (*XRCC4*$^{+/-}$) and used selection in increased G418 concentrations to isolate *XRCC4*$^{-/-}$ clones (Figure 1B). Northern analyses of *XRCC4*$^{-/-}$ ES cell RNA with an *XRCC4* cDNA probe revealed no detectable transcripts (Figure 1C). Therefore, the targeted *XRCC4* mutation appears to represent a null mutation.

XRCC4$^{-/-}$ ES Cells Are Sensitive to IR and Defective in V(D)J Recombination

To determine the effects of the XRCC4 inactivation on DNA damage repair, we first tested the survival of wild-type (wt), *XRCC4*$^{+/-}$, and *XRCC4*$^{-/-}$ ES cells following exposure to IR. These studies showed that *XRCC4*$^{-/-}$ cells, similar to *Ku70*$^{-/-}$ ES cells, had greatly reduced survival compared to wt or *XRCC4*$^{+/-}$ cells (Figure 1D). To determine the impact of XRCC4 deficiency on V(D)J recombination, we assayed the relative ability of *XRCC4*$^{-/-}$ ES cells to support RAG1/2-initiated V(D)J recombination of transiently transfected recombination substrates. These studies showed that XRCC4-deficient ES cells were severely impaired in ability to support formation of both coding and RS joins (Figure 1E). Overall, the XRCC4-deficient ES cells show defects quite similar to those of Ku70-deficient ES cells (Gu et al., 1997a).

XRCC4 Deficiency Results in Late Gestational Lethality

We used two independent *XRCC4*$^{+/-}$ ES clones for germline transmission. *XRCC4*$^{+/-}$ mice appeared indistinguishable from wt littermates; however, we detected no *XRCC4*$^{-/-}$ pups among more than 300 offspring, indicating embryonic lethality. To confirm that embryonic lethality resulted from *XRCC4* inactivation as opposed to some other effect of the inserted PGK-*neo*^{r} cassette, we deleted this cassette in the mouse germline by the *lox*P/Cre recombinase approach (Figure 1A) and confirmed that the homozygous deletion mutation remained embryonic lethal (data not shown). Analyses of *XRCC4*$^{-/-}$ embryos at different gestational stages revealed late gestational lethality at about E16.5 (Table 1). Until E14.5, development of *XRCC4*$^{-/-}$ embryos was grossly normal. However, as gestation proceeded, some *XRCC4*$^{-/-}$ embryos displayed varying degrees of edema (E14.5), and all were significantly runted by E15.5 ($\sim$30% smaller by weight). Dead *XRCC4*$^{-/-}$ embryos first appeared at E14.5 and became much more frequent at E15.5 and E16.5 (Table 1). To date, only two *XRCC4*$^{-/-}$ pups have been delivered, albeit dead.

Growth Defects and Premature Senescence of *XRCC4*$^{-/-}$ Fibroblasts

To investigate the cellular impact of XRCC4 deficiency, we isolated fibroblasts (MEFs) from E13.5 embryos. The doubling time of passage two (P2) *XRCC4*$^{-/-}$ MEFs was about two times longer than that of controls (Figure 2A). Moreover, *XRCC4*$^{-/-}$ MEFs, as compared to *XRCC4*$^{+/-}$ or wt MEFs, displayed accelerated loss of proliferative capacity, failing to undergo further growth after five passages (data not shown). In addition, we observed a markedly reduced ability of *XRCC4*$^{-/-}$ fibroblasts to repair γ-irradiation-generated DSBs as compared to control cells (Figure 2B).

Cell cycle analyses of P3 MEFs revealed significantly fewer cycling cells in *XRCC4*$^{-/-}$ populations (58% for $-/-$; 88% for $+/-$), as judged by bromodeoxyuridine (BrdU) incorporation during a 50 hr labeling period (Figure 2D). Among the noncycling population, roughly 85% were in G0/G1 for both control and mutant MEFs (data

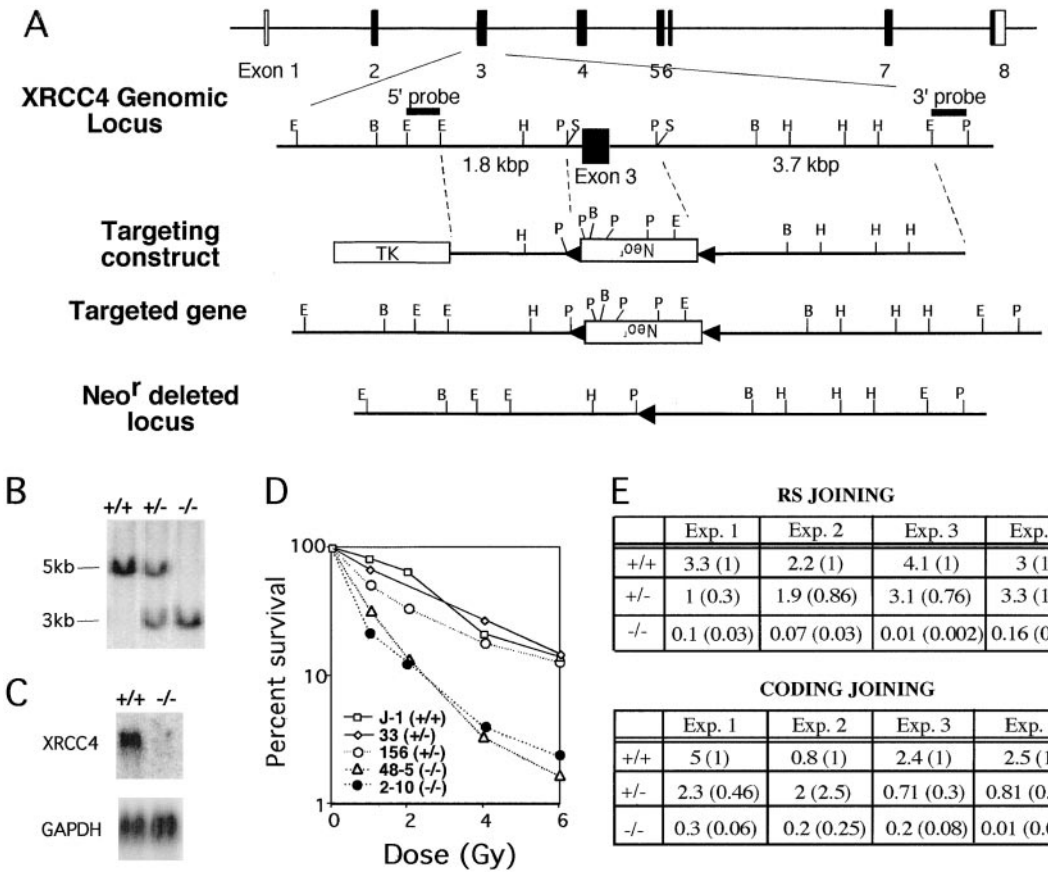

RS JOINING	Exp. 1	Exp. 2	Exp. 3	Exp. 4
+/+	3.3 (1)	2.2 (1)	4.1 (1)	3 (1)
+/-	1 (0.3)	1.9 (0.86)	3.1 (0.76)	3.3 (1.1)
-/-	0.1 (0.03)	0.07 (0.03)	0.01 (0.002)	0.16 (0.05)

CODING JOINING	Exp. 1	Exp. 2	Exp. 3	Exp. 4
+/+	5 (1)	0.8 (1)	2.4 (1)	2.5 (1)
+/-	2.3 (0.46)	2 (2.5)	0.71 (0.3)	0.81 (0.32)
-/-	0.3 (0.06)	0.2 (0.25)	0.2 (0.08)	0.01 (0.004)

Figure 1. *XRCC4* Gene Targeting and Analyses of *XRCC4*$^{-/-}$ ES Cells

(A) Scheme of the *XRCC4* genomic locus and targeting; not to scale. Open boxes, noncoding region of the cDNA; solid boxes, coding sequences; bars, 5′ flanking probe and 3′ flanking probe; Neo′, neomycin-resistance gene; triangles, *lox*P sites; TK, thymidine kinase. Restriction enzymes: E, EcoRI; B, BamHI; P, PstI; S, SacI; H, HindIII.

(B) Representative Southern analysis used to identify targeted allele. BamHI-digested DNA from ES clones was hybridized with the 5′ flanking probe indicated in (A). The germline 5 kb and targeted 3 kb bands are indicated.

(C) Northern analysis. Total RNA (30 μg) from ES cells was hybridized with an XRCC4 cDNA probe (nucleotides 432–726, downstream of exon 3), and a GAPDH cDNA probe.

(D) IR sensitivity of ES cell clones. Cells were irradiated with indicated doses of X irradiation, cultured for 7 days, and surviving colonies stained and counted. IR sensitivity is expressed as the percentages of surviving colonies over unirradiated controls.

(E) Recombination rates (%) of V(D)J RS and coding joining measured by transient V(D)J recombination assay. Relative levels (in parentheses) are normalized to wt samples. Fidelity of RS joining for wt or *XRCC4*$^{+/-}$ cells is 80%–100% and for *XRCC4*$^{-/-}$ is 0%.

not shown). To determine cell cycle kinetics, BrdU pulse-labeled cells were monitored through cell cycle stages during a 28 hr chase period. The cycling *XRCC4*$^{-/-}$ population exhibited similar cell cycle kinetics to controls (Figure 2C). Normal cells respond to DNA damage by activating two major cell cycle checkpoints, G1/S and G2/M. Both checkpoints were retained in *XRCC4*$^{-/-}$ MEFs, as they remained arrested at G1 or G2/M even

Table 1. Analysis of Embryos from *XRCC4*$^{+/-}$ Crosses

Gestational Age (Days)	Total Fetuses	Resorbed Embryos	Genotyped	Live (Dead) Embryos +/+	+/−	−/−	Observed/Expected *XRCC4*$^{-/-}$ Embryos (%)
13.5	96	11	85	23(1)	45	17	80%
14.5	61	5	56	20	27	8(1)	57%
15.5	135	17	118	28	61	14(15)	47%
16.5	175	41	134	35(1)	75(2)	11(13)	33%
20.5 (Birth)	>300	N/A	>300	—	—	0(2)	0%

Genotypes of embryos undergoing maternal resorption were not available. Nonresorbed embryos were genotyped by Southern analysis of their yolk sac DNA. The number of dead embryos is shown in parentheses. Expected Mendelian numbers were determined based on the number of genotyped embryos. N/A, nonapplicable. +/+, +/−, and −/− refer to *XRCC4*$^{+/+}$, *XRCC4*$^{+/-}$, and *XRCC4*$^{-/-}$.

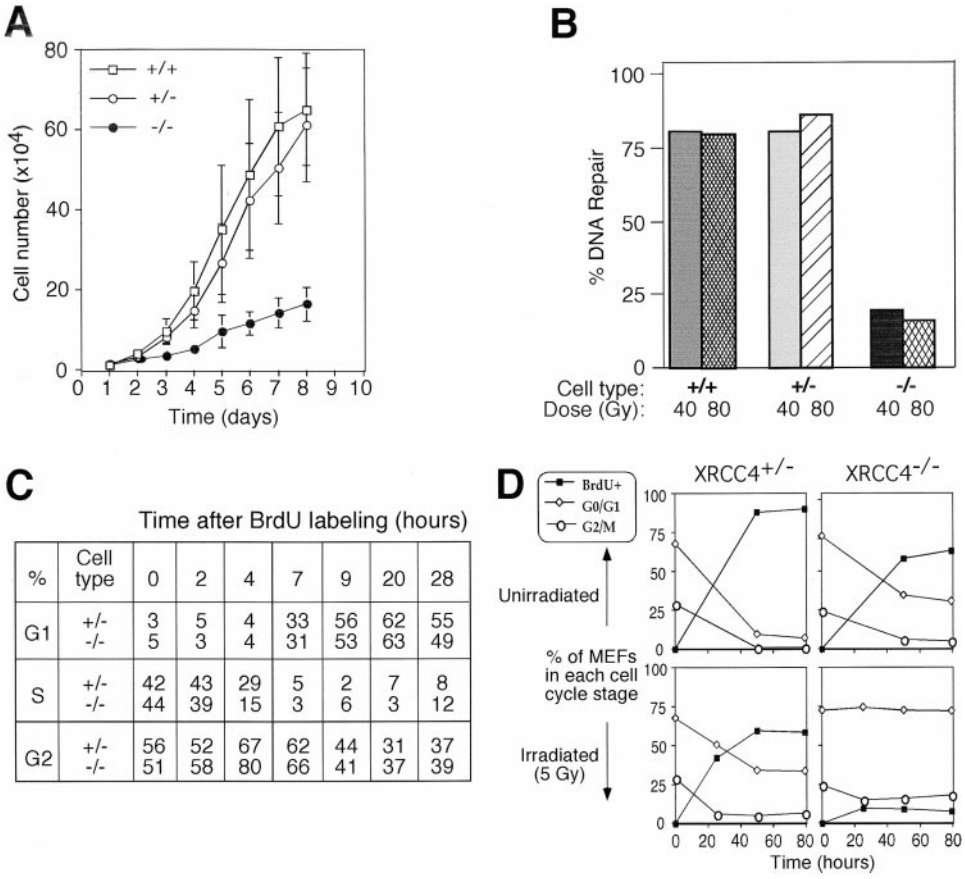

%	Cell type	0	2	4	7	9	20	28
G1	+/-	3	5	4	33	56	62	55
	-/-	5	3	4	31	53	63	49
S	+/-	42	43	29	5	2	7	8
	-/-	44	39	15	3	6	3	12
G2	+/-	56	52	67	62	44	31	37
	-/-	51	58	80	66	41	37	39

Figure 2. Analyses of *XRCC4*$^{-/-}$ Embryonic Fibroblasts

(A) Growth rates of MEFs. Passage 2 (P2) MEFs (from at least four embryos of each genotype) were plated at 10^4/well in 6-well plates and counted every 24 hr.

(B) DSBR capacity in MEFs. Cells were exposed to 40 or 80 Gy of γ-irradiation and allowed to repair for 2 hr before the DNA was analyzed for DSBs. Percentages of repaired DSBs are shown.

(C) Cell cycle kinetics of MEFs. Asynchronous P4 MEFs were pulsed with BrdU for 30 min, and the BrdU-labeled cells were analyzed at the indicated times. Percentages of G1, G2/M, and S phase cells among total live BrdU$^+$ cells are shown.

(D) Intact IR-induced cell cycle checkpoint control in *XRCC4*$^{-/-}$ MEFs. Asynchronous P3 MEFs were irradiated (5 Gy) and then cultured in the presence of BrdU before analysis of cell cycle profile and BrdU incorporation at indicated times by FACS. Percentages among total live cells for each cell cycle stage are shown.

80 hr after γ-irradiation in asynchronous cultures, while control MEFs resumed cycling within 20 hr (Figure 2D). In addition, BrdU pulse-chase experiments showed that irradiated *XRCC4*$^{-/-}$ S phase cells (P3) permanently arrested at the G2/M checkpoint (data not shown).

Together, these studies show that *XRCC4*$^{-/-}$ cells have normal cell cycle checkpoints and suggest that the increase in apparent doubling time of *XRCC4*$^{-/-}$ cultures may result from permanent arrest of *XRCC4*$^{-/-}$ cells at normal DNA damage checkpoints due to inability to efficiently repair DSBs. In addition, these results show that *XRCC4*$^{-/-}$ cells have similar radiosensitivity during the cell cycle to Ku-deficient cells, in contrast to XR-1 mutant CHO cells that are relatively resistant to IR at the late S and early G2 phases (Stamato et al., 1983).

Defective Lymphocyte Development in *XRCC4*$^{-/-}$ Embryos

To determine whether XRCC4 is required for V(D)J recombination in vivo, we first examined fetal thymocyte development. Thymi from *XRCC4*$^{-/-}$ embryos (E16.5) were markedly smaller than those of wt or *XRCC4*$^{+/-}$ littermate controls with total thymocyte numbers reduced approximately 10-fold (data not shown). T cell development in *XRCC4*$^{-/-}$ embryos was arrested at the CD4$^-$CD8$^-$ (double negative, DN) progenitor stage, the same general stage at which *RAG2*$^{-/-}$ T cell development is arrested (Figure 3A), consistent with inability to form the functional TCRβ rearrangements required to signal the DN to double positive (DP) transition. However, total DN cell numbers in *XRCC4*$^{-/-}$ thymi were also reduced (typically 2- to 3-fold) compared to controls, indicating an additional defect. To characterize this defect, we analyzed the DN compartment for expression of CD44 and CD25. In normal development, Dβ to Jβ rearrangement is initiated at CD44$^+$CD25$^+$ stage with most Vβ to DβJβ rearrangements occurring at the CD44$^-$ CD25$^+$ stage (Shortman et al., 1990; Godfrey et al., 1994; Tourigny et al., 1997). In XRCC4-deficient thymi, total numbers and percentages of the most immature DN

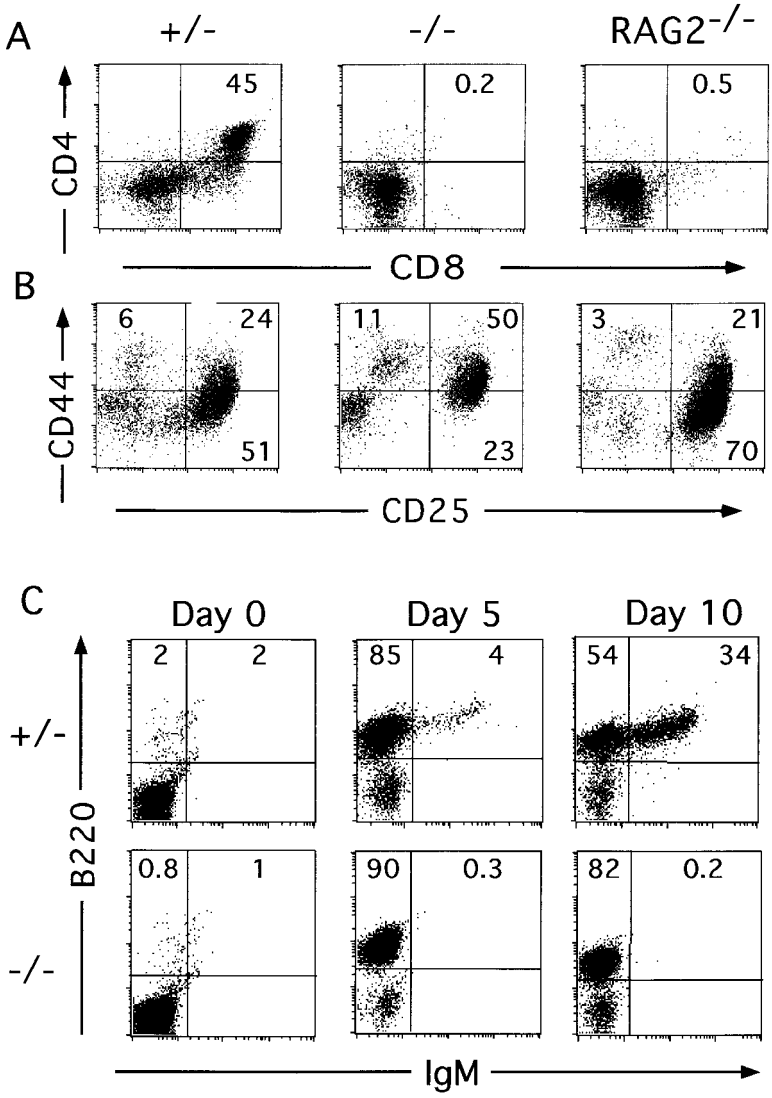

Figure 3. Impaired Development of *XRCC4*$^{-/-}$ Lymphocytes

(A) CD4 and CD8 profile of E16.5 *XRCC4*$^{+/-}$, *XRCC4*$^{-/-}$, and *RAG2*$^{-/-}$ fetal thymocytes.

(B) CD25 and CD44 profile of DN T cells from *XRCC4*$^{+/-}$, *XRCC4*$^{-/-}$, and *RAG2*$^{-/-}$ fetal thymi. E16.5 fetal thymocytes were triple-stained with: (1) an equal titer mixture of cytochrome c–conjugated antibodies against CD4, CD8, CD3, B220, CD19, Gr-1, Mac-1; (2) FITC-anti-CD25; and (3) PE-anti-CD44. Cells negative for the staining in (1) were plotted with CD25 versus CD44.

(C) B220 and IgM profile of cultured fetal liver B cells from *XRCC4*$^{+/-}$ and *XRCC4*$^{-/-}$ embryos. Cultured E15.5 fetal liver pro-B cells were analyzed on day 0, 5, and 10. Percentages of cells in selected quadrants are indicated.

thymocyte populations ($CD44^+CD25^-$ and $CD44^+CD25^+$) were comparable to those of controls, while the number of $CD44^-CD25^+$ DN cells was greatly diminished (Figure 3B). In contrast, all three populations in *RAG2*$^{-/-}$ thymus were similar in numbers to those of controls (Figure 3B). Thus, the XRCC4-deficient phenotype is slightly different than that of RAG deficiency with respect to thymocyte development (see Discussion).

To examine the role of XRCC4 in B cell development, we assayed the ability of mutant and control progenitor B cells from E15.5 fetal livers to expand and differentiate to $B220^+IgM^+$ B cells when cultured on an IL-7-secreting stromal cell line. $B220^+IgM^-$ cells were generated in comparable numbers in *XRCC4*$^{+/-}$ and *XRCC4*$^{-/-}$ samples after 5 days of culture, indicating that expansion and differentiation of *XRCC4*$^{-/-}$ B cell precursors to the $B220^+$ stage were unaffected (Figure 3C). In contrast, no $B220^+IgM^+$ cells appeared in *XRCC4*$^{-/-}$ cultures even after 10 days, indicating lack of progression beyond the $B220^+IgM^-$ progenitor stage (Figure 3C), reminiscent of the block in B cell development observed in the context of RAG deficiency (Mombaerts et al., 1992; Shinkai et al., 1992). However, *XRCC4*$^{-/-}$ pro-B cells, unlike RAG-deficient pro-B cells, attempt to perform V(D)J recombination, as PCR analyses allowed recovery of $V_H(D)J_H$ joining events from *XRCC4*$^{-/-}$ fetal liver cultures that had aberrant deletions from one or both participating coding gene segments (see supplemental figure on *Cell* website [http://www.cell.com/cgi/content/full/95/26/891/DC1]). In addition, Abelson murine leukemia virus (A-MuLV) transformants derived from cultured *XRCC4*$^{-/-}$ pro-B cells had large deletions spanning their J_H locus (data not shown), similar to those observed in SCID A-MuLV transformants (Malynn et al., 1988).

Massive Neuronal Cell Death in *XRCC4*$^{-/-}$ Embryos

The defects in lymphocyte development cannot account for the embryonic lethality associated with XRCC4 deficiency. To identify specific pathological change(s) in mutant embryos that might cause embryonic death, we performed histological analyses on *XRCC4*$^{-/-}$ embryos

and littermate controls. Although some *XRCC4*$^{-/-}$ embryos developed edema by E14.5, histological serial sections revealed no obvious cardiovascular defect, nor did microdissection of mutant hearts (E15.5) reveal structural abnormalities (data not shown). In addition, hemorrhages were not evident in live mutant embryos at any stage examined (E10.5–E16.5). We also looked for signs of defective hematopoietic development by cytological analyses of peripheral blood and fetal liver cells from E14.5 embryos and found definitive erythrocytes, megakaryocytes, and myeloid cell lineages to be comparable to wt controls (data not shown).

Strikingly, the only abnormality we observed among all tissues examined histologically was severe cell death throughout the developing central nervous system (CNS) and peripheral sensory ganglia, including the dorsal root ganglia (Figures 4a–4f and data not shown). During normal embryonic neurodevelopment, significant levels of apoptosis occur in wt animals, and this programmed cell death is believed to be essential for determining the cytoarchitecture of the brain (Datta and Greenberg, 1998). However, we observed a significantly larger number of densely staining, pyknotic nuclei (a morphological indicator of cell death) in hematoxylin-eosin (HE) stained sections of *XRCC4*$^{-/-}$ embryonic CNS, compared to those of controls (Figures 4b and 4c versus 4e and 4f; other data not shown). In some areas, the level of *XRCC4*$^{-/-}$ cell death was so massive that it resulted in severe acellularity, as manifested, for example, by a cavity within the intermediate zone (IZ) of *XRCC4*$^{-/-}$ cerebral hemispheres (Figure 4d). In normal mice, mitotic neuronal progenitors reside in the ventricular zone (VZ) of the developing CNS. These progenitors give rise to neurons that exit the cell cycle and migrate through the mantle layer (ML) where they differentiate. Strikingly, the massive apoptotic death throughout the developing CNS of *XRCC4*$^{-/-}$ mice was localized to the ML; in contrast, the VZ appeared indistinguishable between mutants and controls (Figures 4b and 4c versus 4e and 4f).

To confirm the neuronal identity of the dead cells in the *XRCC4*$^{-/-}$ CNS, we stained embryonic sections simultaneously with antibodies against β3-tubulin (specific for postmitotic neurons) and nestin (specific for neuroprogenitors), in addition to the nuclear stain Hoechst (Figures 5a–5e). In these assays, cells with pyknotic nuclei resided within the anti-β3-tubulin-positive population and not in the nestin-positive cell population (Figures 5b–5e). This staining data, together with the anatomical location of the increased numbers of apoptotic cells, confirmed that the massive cell death observed in mutants was in postmitotic neuronal populations, while proliferative progenitors were spared. Furthermore, the anti-nestin-positive progenitor cells appeared restricted to the VZ both in wt and *XRCC4*$^{-/-}$ animals (Figure 5a and data not shown), indicating that XRCC4 deficiency does not lead to aberrant migration of neuroprogenitor cells away from the VZ. In addition, a 1–3 hr BrdU pulse-labeling experiment of *XRCC4*$^{-/-}$ embryos showed that mitotic cells were confined to the VZ (as in wt) and that cells in the ML exhibited no obvious aberrant replication (data not shown). Finally, we performed TUNEL (terminal deoxynucleotidyl transferase–mediated dUTP biotin nick end labeling) to assay for nuclear DNA fragmentation and detected greatly increased numbers of TUNEL stain-positive nuclei in *XRCC4*$^{-/-}$, as opposed to control brain sections (Figures 5f and 5g; medullar region of the hindbrain), consistent with the increased cell death occurring via an apoptotic process.

Neuronal Cell Death in *XRCC4*$^{-/-}$ Embryos Correlates with the Temporal and Spatial Pattern of Neuronal Generation

The generation of neuronal cells in the CNS is spatially and temporally controlled, starting at cervical regions of the neurotube (E10.5), extending caudally to the sacral cord, and rostrally through the hindbrain (E11) and midbrain (E11) to the forebrain (E11–12). Within the spinal cord, neurogenesis also follows a ventral to dorsal gradient, such that ventral portions of the spinal cord begin neurogenesis earlier (E9–10) than the dorsal portions (E11) (Nornes and Carry, 1978). Likewise, in normal development, the cessation of neurogenesis in these CNS regions generally follows a similar sequence to their onset (Bayer and Altman, 1991).

In *XRCC4*$^{-/-}$ mutants, abnormal levels of dead cells first appeared in the ventral portions of the spinal cord at E10.5, parallel with the initiation of neurogenesis in this region (E10), while appearance of apoptosis in the dorsal portions of the spinal cord began at E11.5, also following the onset of neurogenesis (data not shown). Portions of the hindbrain became affected at E11.5, midbrain and diencephalon at E12.5, and the cerebral cortex at E13.5 (Figure 6). Furthermore, neurogenesis in normal cortex starts at E11 ventrolaterally and E12 dorsalmedially, peaks around E12.5 and E13.5 (ventrolaterally and dorsalmedially, respectively), and continues at lower levels until E18 (Bayer and Altman, 1991); correspondingly, we observed peak cell death in *XRCC4*$^{-/-}$ cerebral cortices at E13–14 ventrolaterally and E14–15 dorsalmedially (Figure 6 and data not shown). At E16.5 (the latest stage examined), pyknosis was mild in the mutant cortex; although the cavity in the IZ of cerebral hemispheres, first seen at E13.5, was still present, and the cortical plate remained thin (Figures 4d and 4e; data not shown). This apparent temporal correlation between neuronal development and abnormal apoptosis in *XRCC4*$^{-/-}$ embryos was further substantiated by the disappearance of pyknosis in specific brain regions at defined gestational ages. For example, neurogenesis in the hindbrain ceases before E14 (Nornes and Carry, 1978); correspondingly, no obvious pyknosis was observed in the *XRCC4*$^{-/-}$ hindbrain after E14.5 (Figure 6l).

Overall, these studies show that the increased cell death in specific regions of the *XRCC4*$^{-/-}$ CNS is closely linked to the onset and cessation of neurogenesis in a particular region. In addition, our finding that detectable apoptosis diminishes after neurogenesis in *XRCC4*$^{-/-}$ embryos further supports our findings that most of the increased cell death involves early postmitotic neurons and not mature neurons.

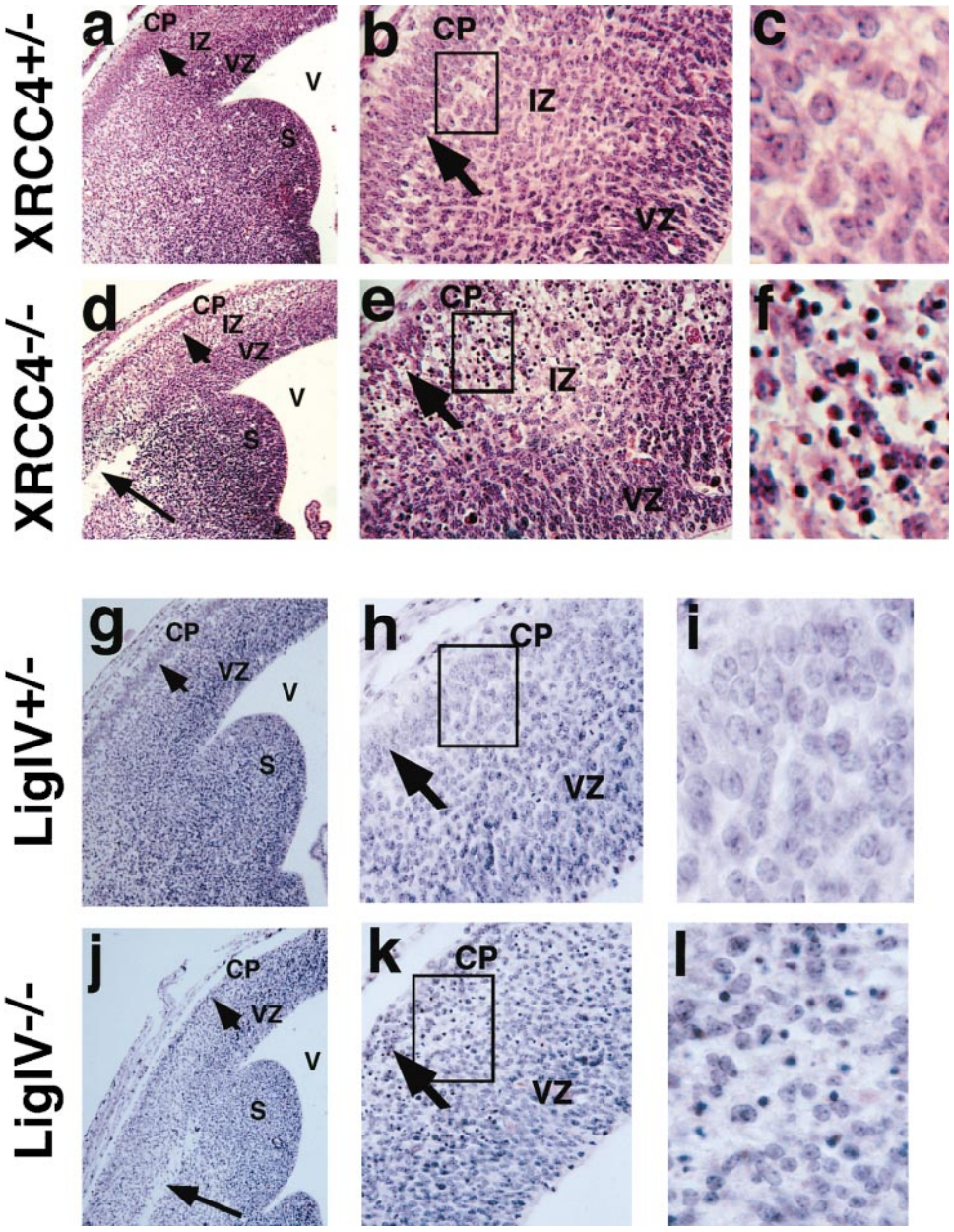

Figure 4. Massive Cell Death in Postmitotic Regions of *XRCC4*$^{-/-}$ and *LigIV*$^{-/-}$ CNS

(a–f) Hematoxylin and eosin (HE) staining of littermate *XRCC4*$^{+/-}$ and *XRCC4*$^{-/-}$ brain sections. Horizontal brain sections of E14.5 *XRCC4*$^{+/-}$ (a–c) and *XRCC4*$^{-/-}$ (d–f) mutants at a comparable level reveal severe acellularity (cavitation, long arrow) and thinner cortical plate (small arrows) in the cerebral hemisphere of *XRCC4*$^{-/-}$ brain. Higher magnifications show relatively normal VZ of the mutant cortex ([a] and [b] vs. [d] and [e]), whereas in the IZ extending to the cortical plate there are numerous pyknotic nuclei (dense hematoxylin stain) (e and f).

(g–l) HE staining of littermate *LigIV*$^{+/-}$ *and LigIV*$^{-/-}$ brain sections. Coronal sections of E13.5 control *LigIV*$^{+/-}$ (g–i) and *LigIV*$^{-/-}$ (j–l) brains reveal similar defects in *LigIV*$^{-/-}$ cerebral hemisphere to those observed in *XRCC4*$^{-/-}$ mutant. V, lateral ventrical; C, cortex; S, striatum; VZ, ventricular zone; IZ, intermediate zone; CP, cortical plate. Boxed areas in (c) and (e), and (i) and (k) are enlarged in (d) and (f), and (j) and (l) by image processing. Original magnifications: (a, d, g, and j), 100×; (b, c, e, f, h, i, k, and l), 400×.

Neuronal Cell Death in *Ligase IV*$^{-/-}$ Embryos

We have recently generated *Lig IV*$^{-/-}$ mice and demonstrated that they have an identical phenotype to XRCC4-deficient mice with respect to impaired V(D)J recombination, IR sensitivity, cellular growth defects, and embryonic lethality (Frank et al., 1998). To determine whether the effects of XRCC4 deficiency on neurogenesis also could be explained in the context of functional association with ligase IV, we assayed for potential CNS lesions in *Lig IV*$^{-/-}$ embryos. Examination of HE-stained sections from ligase IV–deficient embryos revealed similar CNS defects to those observed in the *XRCC4*$^{-/-}$ CNS. For

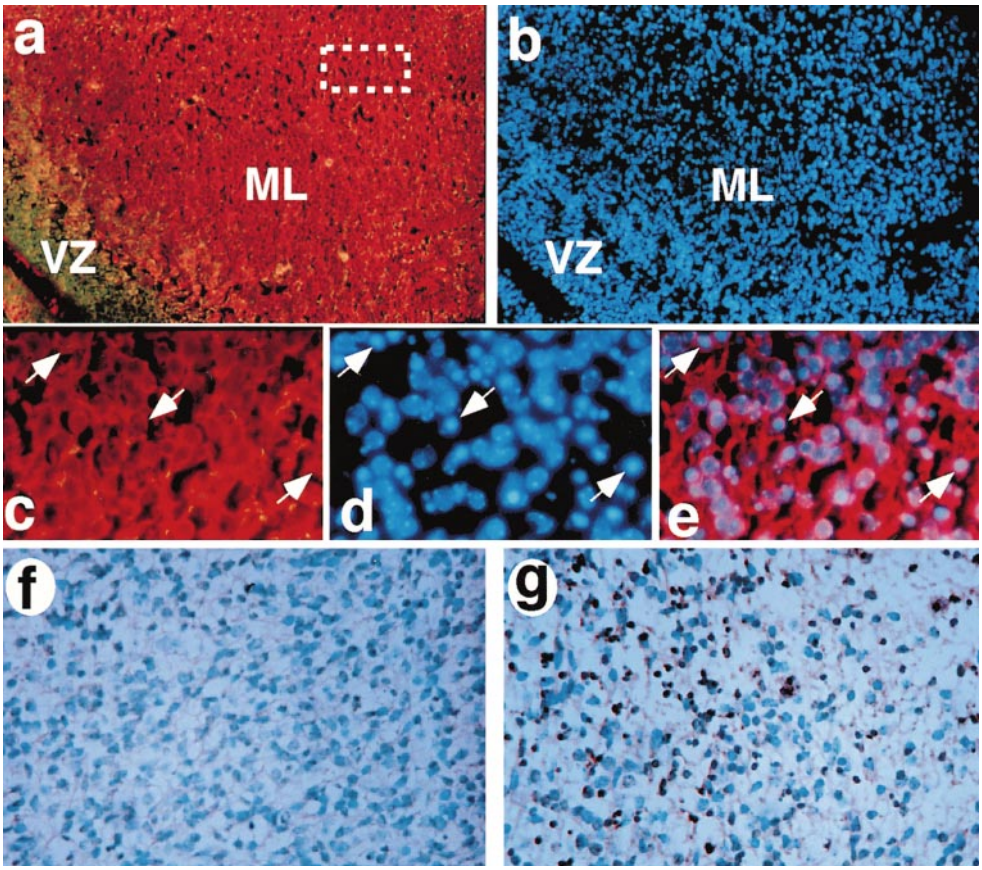

Figure 5. Massive Cell Death Occurs in *XRCC4*$^{-/-}$ Postmitotic Neurons by Apoptosis

(a–e) Areas of the hindbrain in sagittal sections (E12.5) stained with TuJ1 (anti-β3-tubulin antibody, red), anti-nestin antibody (green), and nuclear stain Hoechst (blue). (a) Under low magnification, the anti-nestin-positive progenitor layer (VZ) and the TuJ1-positive neuronal layer (ML) remain distinct in mutant samples (double exposure for TuJ1 and anti-nestin stains). However, Hoechst staining (blue) reveals numerous pyknotic nuclei (dense, bright blue) in the ML (b), although densely populated nuclei in the VZ exhibit normal diffuse blue staining ([b], in VZ). Under higher magnification of boxed area in (a), pyknotic nuclei stained by Hoechst (arrows in [d]) are identified as belonging to TuJ1-positive neuronal cells (arrows in [c], double exposure of TuJ1 and anti-nestin stains; and [e], double exposure of TuJ1 and Hoechst). VZ, ventricular zone; ML, mantle layer.

(f and g) TUNEL assay on *XRCC4*$^{+/+}$ control (f) and *XRCC4*$^{-/-}$ (g) hindbrain sections. Areas of the hindbrain in sagittal sections (E12.5) stained with TUNEL labeling agents. Original magnifications: (a and b), 200×; (c–g), 400×; (c–e), enlarged by image processing.

example, coronal sections of E13.5 *Lig IV*$^{-/-}$ cortex exhibit an abnormally high number of pyknotic nuclei and acellularity resulting in an aberrant cavity (Figures 4g–4l).

Discussion

XRCC4 deficiency in cells results in proliferation defects, DSBR defects, and inability to support either the coding or RS end-joining processes required to complete the V(D)J recombination reaction. These defects are quite similar to those observed with Ku- and ligase IV–deficient cells and likely result from impairment of an end-joining reaction that employs all of these proteins. However, XRCC4, in contrast to Ku, is required for normal embryonic development, with XRCC4-deficient embryos dying over a relatively broad period in late gestation. Analyses of the mutant embryos revealed defects only in lymphocyte and neuronal development; massive apoptotic cell death of newly generated, postmitotic neurons was the only potential cause of death identified. Strikingly, ligase IV deficiency results in similar neuronal developmental defects. Therefore, this neuronal death phenotype almost certainly results from the absence of a shared XRCC4 and ligase IV function.

Differential Requirements for XRCC4/Ligase IV Versus Ku Proteins

It is curious that the embryonic lethality and severe neuronal developmental abnormalities observed in XRCC4- and ligase IV–deficient mice were not observed in Ku70/80-deficient mice, given that they all share similar cellular growth and V(D)J recombination defects. Two possible scenarios can be envisioned to explain these differences. One is that XRCC4 and ligase IV have evolved additional functions in end joining or other reactions, perhaps in association with other proteins. A second, likely possibility is that the less severe developmental defects of Ku-deficient mice result from a higher residual

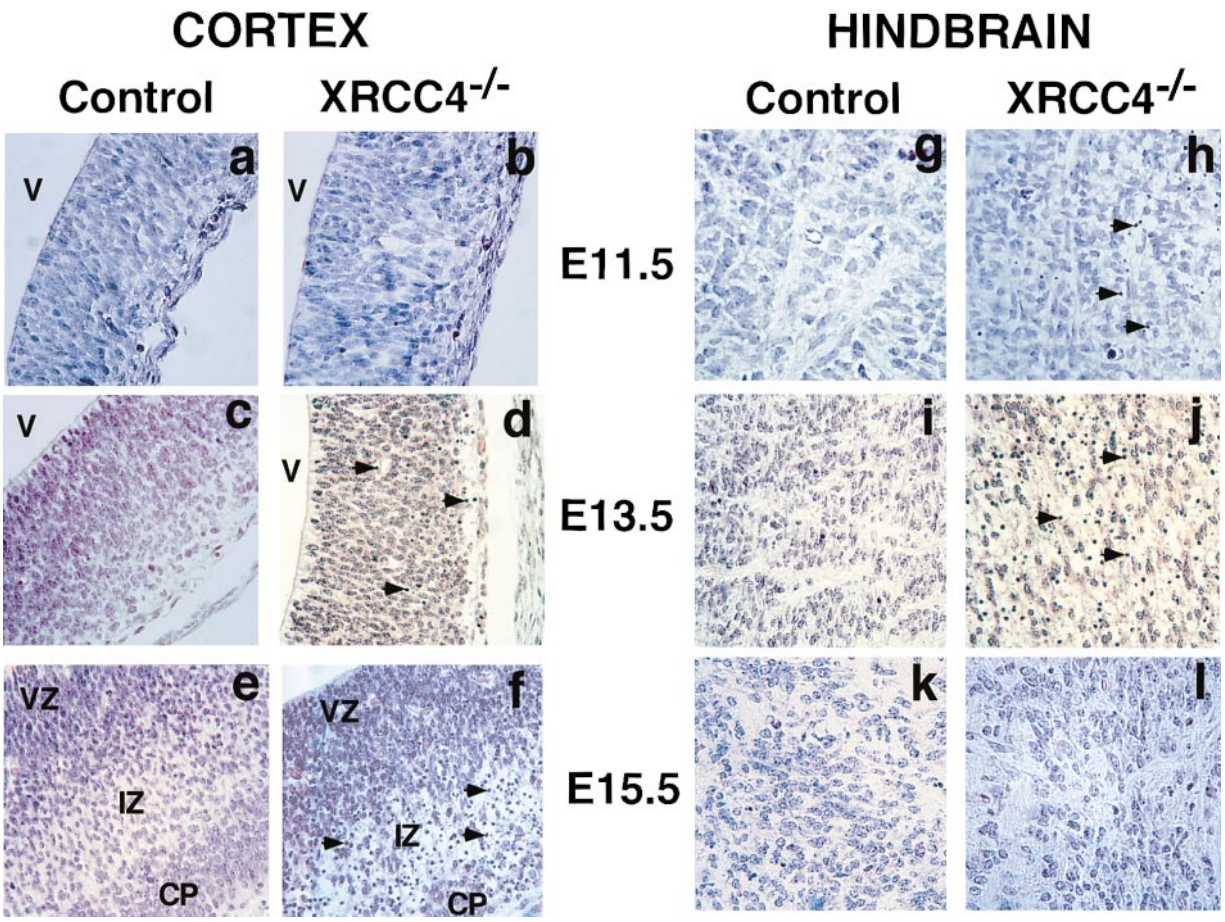

Figure 6. Neuronal Death in XRCC4-Deficient Embryos Correlates with Temporal and Spatial Patterns of Neurogenesis

Regions of the dorsalmedial cortex (or precortex) (a–f) and hindbrain (g–l) in sagittal sections of control (either wt or *XRCC4*$^{+/-}$) (a, c, e, g, i, and k) and *XRCC4*$^{-/-}$ (b, d, f, h, j, and l) littermate embryos at indicated developmental stages (E11.5, E13.5, E15.5) were stained with HE. Arrowheads indicate apoptotic nuclei. V, lateral ventrical; VZ, ventricular zone; IZ, intermediate zone; CP, cortical plate. Original magnification, 400×.

level of "leaky" end joining in Ku-deficient cells than in XRCC4/ligase IV–deficient cells. In this regard, it is notable that *Ku70*$^{-/-}$ mice show a partial depletion of enteric neurons (Li et al., 1998), which may well be a milder manifestation of the massive neuronal death observed in the context of XRCC4 and ligase IV deficiencies.

Essential Role of XRCC4 in Lymphocyte Development

XRCC4-deficient ES cells exhibit almost no ability to complete the formation of RAG-initiated coding or RS joins in a transient V(D)J recombination assay (Figure 1E). Correspondingly, *XRCC4*$^{-/-}$ B and T cell development is blocked at the early progenitor stage in which V(D)J recombination is initiated. In progenitor B lineage cells, rare joins of RAG-cut IgH loci generated in the absence of XRCC4 contain large junctional deletions that range from within normal limits to several kilobases or more. Similar aberrant recombination events attributed to low-level secondary recombination pathways in SCID pro-B cell lines are thought to be selected due to a survival advantage at the cellular level (Malynn et al., 1988). In addition, we detected similar levels of RS ends in *XRCC4*$^{-/-}$, *Ku70*$^{-/-}$, and SCID thymocytes (data not shown), suggesting that RS cleavage is normal in *XRCC4*$^{-/-}$ developing thymus. Together, these results demonstrate an essential role of XRCC4 for the end-joining steps of the V(D)J recombination reaction in vivo.

By analogy to Ku-deficient or DNA-PKcs deficient (SCID) progenitor lymphocytes, there are likely two related, but distinct, mechanisms by which XRCC4 deficiency leads to impaired lymphogenesis. One is the inability to make functional antigen receptor gene rearrangements needed to generate the Ig or TCR chains that signal expansion and further differentiation of progenitor B and T cells, similar to that associated with RAG1/2 deficiency. However, a second is demonstrated by the absence in XRCC4-deficient fetal thymi, but not in RAG-deficient fetal thymi, of early progenitor T lineage populations in which TCRβ loci become accessible for V(D)J recombination. This absence is consistent with a probable survival defect of XRCC4-deficient progenitor lymphocytes that fail to repair RAG-initiated DSBs at Ig or TCR loci, a phenomenon well-documented in SCID mice where lymphocyte development is impaired even in the presence of functional antigen receptor genes (Kishi et al.,

1991; Shinkai et al., 1992; Chang et al., 1995). A similar death of activated mature B cells attempting to undergo CSR has been proposed in the context of Ku deficiency (Casellas et al., 1998; Manis et al., 1998).

XRCC4 and DNA Ligase IV Play an Essential Role in the Development of the Nervous System

In addition to defects in the lymphoid system, the only other defect we observed, so far, in *XRCC4*$^{-/-}$ and *LigIV*$^{-/-}$ embryos was in the nervous system. During neuronal development, proliferating neuroprogenitor cells exit the cell cycle and differentiate into neurons or glial cells. This developmental program is temporally and spatially controlled throughout the nervous system. In *XRCC4*$^{-/-}$ embryos, an abnormally large number of apoptotic neurons were present in peripheral sensory ganglia and multiple regions of the CNS; however, the increased number of dying cells was limited to newly generated, postmitotic neuronal populations. Furthermore, there was a close temporal relationship between the normal neurogenesis program in a given region and the appearance and disappearance of apoptotic cells. The aberrant increase in cell death in regions of the *XRCC4*$^{-/-}$ CNS occurred in a wave that temporally followed the wave of neurogenesis. This temporal relationship between neurogenesis and apoptosis strongly suggests a limited period of susceptibility closely linked to the point at which the *XRCC4*$^{-/-}$ neuronal precursors become postmitotic neurons.

Potential Causes of Massive Neuronal Death in XRCC4 and DNA Ligase IV–Deficient Embryos

The only known function of XRCC4 and ligase IV are their roles in the end-joining reactions used in general DSBR or V(D)J recombination. Thus, it seems reasonable that the neuronal cell defect in XRCC4- and ligase IV–deficient embryos may be due to an impaired DNA end-joining reaction. In this regard, previous studies of IR sensitivity during rat embryonic cortical development suggested highest sensitivity immediately after the birth of a neuron (Bayer and Altman, 1991). As this period appears to coincide with the wave of abnormal cell death in *XRCC4*$^{-/-}$ neuronal cells during cortical development, it further supports the possibility that massive death of newly generated *XRCC4*$^{-/-}$ and *ligase IV*$^{-/-}$ neurons may result from a particular sensitivity to excess DSBs, which cannot be efficiently repaired in the absence of these factors.

It also remains possible that excessive postmitotic neuronal death in XRCC4/ligase IV–deficient mice might be due to other processes. The pattern of neuronal cell death in *XRCC4*$^{-/-}$ embryos is similar to that observed in pRB-deficient embryos, which die around E14.5 due to additional defects, including hematopoietic defects (Lin et al., 1996). However, massive cell death in the postmitotic regions of the p*RB*$^{-/-}$ CNS is associated with ectopic mitosis, which we do not find in the *XRCC4*$^{-/-}$ CNS. In this regard, XRCC4 deficiency causes premature termination of the replicative cell cycle in MEFs, rather than cell cycle deregulation as observed in the absence of pRB. Another possible explanation for the XRCC4/ligase IV neuronal phenotype of enhanced apoptosis could be absence of, or impaired responses to, exogenous factors, such as trophic molecules released by target cells during formation of synaptic contacts. However, trophic factors are most often important for neuronal survival only at later stages than those affected by XRCC4/ligase IV deficiency. Yet another possibility is that persistence of DSBs or other factors associated with XRCC4/ligase IV deficiency might force premature entry of neurons into a postmitotic stage that leads to premature differentiation, ultimately leading to death. However, this also appears unlikely because the temporal control of CNS development was normal in *XRCC4*$^{-/-}$ embryos; furthermore, there were no apparent signs of premature neurogenesis.

Overall, our findings are most consistent with increased death of early postmitotic neurons in XRCC4/ligase IV–deficient embryos due to increased occurrence of unrepaired DSBs. In this context, the neuronal death phenotype of XRCC4 and ligase IV deficiency is strikingly similar to that observed in *BclX*-deficient mice, a deficiency that also results in embryonic lethality (Motoyama et al., 1995). *BclX* is a survival gene and a member of the Bcl2 family (Merry and Korsmeyer, 1997). Although *BclX*-deficient embryos have several additional defects, one of the most well defined is increased death of immature lymphocytes, providing an additional similarity in the *BclX* and XRCC4/ligase-IV deficient phenotypes. In the latter context, various studies have suggested that *BclX* expression is required in developing B and T lymphocytes to support cell survival during the period of antigen receptor gene rearrangement (Behrens and Mueller, 1997). Overall, the similarities in the lymphoid and neuronal defects in *BclX*-deficient and XRCC4/ligase IV–deficient mice are compatible with the notion that affected neuronal cells in these mutants die, respectively, from increased sensitivity to DSBs and inability to repair DSBs. Finally, Northern analyses of total RNA from normal embryonic cortex revealed XRCC4 expression but showed no obvious differences in levels compared to other embryonic regions at different developmental stages (data not shown). While more detailed analyses need to be done, this expression pattern is consistent with the notion that XRCC4 is involved in repair of DSBs that arise (either nonspecifically or specifically) in all cell types (Li et al., 1995).

Potential Sources of DSBs in Postmitotic Neurons

What is the source of the DSBs that appear to lead to widespread death of newly generated, postmitotic XRCC4/ligase IV–deficient neurons? One possibility is that these breaks represent basal levels generated nonspecifically by normal metabolism of all cells, but that particular neuronal cells are much more sensitive to their presence. Another possibility is an elevated level of nonspecific DSBs due to altered cellular conditions associated with the affected period of neuronal differentiation. A third, intriguing alternative is that DSBs could be generated by a specific neuronal process, such as a recombination process, required for neuronal differentiation/function (Chun and Schatz, 1993). In this context, several studies of DSBs and cell death in the embryonic

CNS continue to raise the notion of parallels with lymphocyte-specific processes (Blaschke et al., 1998). The possibility of recombination in the CNS gained wide recognition from the finding of RAG1 expression in postmitotic regions of the embryonic CNS (Chun et al., 1991), although no CNS phenotype has been described for RAG1-deficient mice. In this regard, however, it would seem likely that any specific process potentially involving a DSB outside of lymphocytes might be initiated by a novel enzyme and completed by the common DSBR machinery. Whatever the source of the DSBs that appear to cause defective neurogenesis in XRCC4/ligase IV–deficient embryos, our studies have clearly outlined the general stage of neuronal development in which such breaks occur.

Experimental Procedures

Generation of *XRCC4*$^{-/-}$ Mice

A targeting construct was made to replace exon 3 (nucleotides 218–393 of the *XRCC4* cDNA) with a neomycin resistance gene. J1 (kindly provided by R. Jaenisch) and E14.1 (kindly provided by R. Murray) ES cells were transfected and selected as described (Kuhn et al., 1991). Homologous recombinants were verified by Southern analyses using 5′ and 3′ external probes, and the neo^r probe. *XRCC4*$^{+/-}$ ES cells were injected into C57Bl/6 blastocysts to generate chimeras that were backcrossed with C57Bl/6 mice for germline transmission. To generate mice with neo^r-deleted mutant alleles, heterozygous mutant mice were bred with EIIA-Cre/CD1 mice (Lakso et al., 1996). Two independent *XRCC4*$^{+/-}$ clones (J1) were subjected to higher concentrations of G418 selection to generate *XRCC4*$^{-/-}$ subclones. ES cell IR sensitivity was tested by a colony survival assay (Gu et al., 1997a), and transient V(D)J recombination assays were performed as described (Taccioli et al., 1993).

Histological Analysis

Embryos were fixed in Bouin's solution or 4% paraformaldehyde, paraffin embedded, serially sectioned (5 μm), and stained with hematoxylin and eosin. TUNEL was performed on paraformaldehyde-fixed sections using DNA Fragmentation Detection kit (CAL Biochem). Immunostaining of paraformaldehyde-fixed sections was performed using rabbit anti-nestin and monoclonal anti-β3-tubulin antibodies, followed by CY2-coupled goat anti-rabbit and CY3-coupled goat anti-mouse secondary antibodies (Jackson laboratory). Nuclei were counterstained with Hoechst.

Preparation and Analyses of MEFs

MEFs isolated from E13.5 embryos were designated passage 0 (P0), and subsequent passages as P1, P2, etc., when split at 1:5. Growth rates and proliferation capacity were determined as described (Gu et al., 1997b). DSBR was analyzed by asymmetric field inversion gel electrophoresis (AFIGE) as described (Stamato et al., 1993).

Cell Cycle Analysis

Asynchronous MEF cultures were pulse-labeled in medium containing 10 μM BrdU (Sigma) and then cultured in the absence of BrdU at 2×10^5 cells/well in 6-well plates, or were continuously labeled in BrdU containing medium (65 μM), then harvested at indicated times as described (Gu et al., 1997b). For irradiation studies, MEFs were irradiated at a ^{137}Cs source with 5 Gy. Cells were stained with FITC-anti-BrdU (Becton Dickinson) and propidium iodide (PI) (Sigma) as per the Becton Dickinson protocol. Samples were collected on a FACS Caliber flow cytometer (Becton Dickinson) using CellQuest software (Becton Dickinson) and analyzed using FlowJo software (Tree Star, Inc., San Carlos, CA). Percentages of MEFs in each cell cycle stage were determined based on the PI/anti-BrdU staining pattern for live cells.

Analyses of Fetal Lymphocytes

Single-cell suspensions of fetal thymi were stained with anti CD3 (145-2C11), B220 (RA3-6B2), CD19 (1D3), Gr-1 (RB6-8C5), Mac-1 (M1/70), CD25 (7D4), CD44 (IM7), CD8 (53-6.7), and CD4 (GK1.5) antibodies (Pharmingen, Southern Biotechnology Associates) conjugated with fluorescein isothiocyanate (FITC), cytochrome c, or phycoerythrin (PE). Fetal liver cultures on T220 stromal cells (from Gary Borzillo) were stained with anti-IgM-FITC (goat anti-mouse polyclonal) and anti-B220-PE (clone RA3–6B2) antibodies (Pharmingen, Southern Biotechnology Associates) as described (Frank et al., 1998).

Acknowledgments

We thank Milton Datta, Landy Kangaloo, Cecilia Lundberg, André Choulika, Jerold Chun, David Weaver, and Ronald DePinho for advice or assistance. The work was supported by the Howard Hughes Medical Institute, by National Institutes of Health grants A.I.20047 and A.I.35714 (F. A.), A.I.01428 (K. F.), C.A.61009 (B. M.), and GM50718 (G. R.), and by fellowships from the Damon Runyan Cancer Research Fund (Y. G. and J. C.), the Cancer Research Institute (C. Z.), the Life Sciences Research Foundation (K. F.), and the Leukemia Society of America (J. S.).

Received October 19, 1998; revised November 6, 1998.

References

Bayer, S.A., and Altman, J. (1991). Neocortical development. (New York: Raven Press).

Behrens, T.W., and Mueller, D.L. (1997). Bcl-x and the regulation of survival in the immune system. Immunologic Res. *16*, 149–160.

Blaschke, A., Weiner, J., and Chun, J. (1998). Programmed cell death is a universal feature of embryonic and postnatal neuroproliferative regions throughout the central nervous system. J. Comp. Neurol. *396*, 39–50.

Casellas, R., Nussenzweig, A., Wuerffel, R., Pelanda, R., Reichlin, A., Suh, H., Qin, X.F., Besmer, E., Kenter, A., Rajewsky, K., and Nussenzweig, M.C. (1998). Ku80 is required for immunoglobulin isotype switching. EMBO J. *17*, 2404–2411.

Chang, Y., Bosma, G.C., and Bosma, M.J. (1995). Development of B cells in scid mice with immunoglobulin transgenes: implications for the control of V(D)J recombination. Immunity *2*, 607–616.

Chu, G. (1997). Double strand break repair. J. Biol. Chem. *272*, 24097–24100.

Chun, J.M., and Schatz, D.G. (1993). Recombination activation gene-1 (RAG-1) transcription in the mammalian CNS. In Neuronal Cell Death and Repair, A.C. Cuello, ed. (Amsterdam, NY: Elsevier Science Publishers B.V.), pp. 283–295.

Chun, J.J., Schatz, D.G., Oettinger, M.A., Jaenisch, R., and Baltimore, D. (1991). The recombination activating gene-1 (RAG-1) transcript is present in the murine central nervous system. Cell *64*, 189–200.

Critchlow, S., Bowater, R., and Jackson, S. (1997). Mammalian DNA double-strand break repair protein XRCC4 interacts with DNA ligase IV. Curr. Biol. *7*, 588–589.

Datta, S.R., and Greenberg, M.E. (1998). Molecular mechanisms of neuronal survival and apoptosis. Hormones and Signaling *1*, 94–103.

Errami, A., Smider, V., Rathmell, W.K., He, D.M., Hendrickson, E.A., Zdzienicka, M.Z., and Chu, G. (1996). Ku86 defines the genetic defect and restores X-ray resistance and V(D)J recombination to complementation group 5 hamster cell mutants. Mol. Cell. Biol. *16*, 1519–1526.

Frank, K.M., Sekiguchi, J.M., Seidl, K.J., Swat, W., Rathbun, G.A., Cheng, H.-L., Davidson, L., Kangaloo, L., and Alt, F.W. (1998). Late embryonic lethality and impaired V(D)J recombination in mice lacking DNA ligase IV. Nature *396*, 173–177.

Gao, Y., Chaudhuri, J., Zhu, C., Davidson, L., Weaver, D., and Alt,

F. (1998). A targeted DNA-PKcs-null mutation reveals DNA-PK-independent functions for Ku in V(D)J recombination. Immunity *9*, 367–376.

Gellert, M. (1997). Recent advances in understanding V(D)J recombination. Adv. Immunol. *64*, 39–64.

Godfrey, D.I., Kennedy, J., Mombaerts, P., Tonegawa, S., and Zlotnik, A. (1994). Onset of TCR-beta gene rearrangement and role of TCR-beta expression during $CD3^{-}CD4^{-}CD8^{-}$ thymocyte differentiation. J. Immunol. *152*, 4783–4792.

Grawunder, U., Wilm, M., Wu, X., Kulesza, P., Wilson, T.E., Mann, M., and Lieber, M.R. (1997). Activity of DNA ligase IV stimulated by complex formation with XRCC4 protein in mammalian cells. Nature *388*, 492–495.

Grawunder, U., Zimmer, D., Fugmann, S., Schwarz, K., and Lieber, M.R. (1998). DNA ligase IV is essential for V(D)J recombination and DNA double-strand break repair in human precursor lymphocytes. Mol. Cell *2*, 477–484.

Gu, Y., Jin, S., Gao, Y., Weaver, D.T., and Alt, F.W. (1997a). Ku70-deficient embryonic stem cells have increased ionizing radiosensitivity, defective DNA end-binding activity, and inability to support V(D)J recombination. Proc. Nat. Acad. Sci. USA *94*, 8076–8081.

Gu, Y., Seidl, K.J., Rathbun, G.A., Zhu, C., Manis, J.P., van der Stoep, N., Davidson, L., Cheng, H.-L., Sekiguchi, J., Frank, K., et al. (1997b). Growth retardation and leaky SCID phenotype of Ku70-deficient mice. Immunity *7*, 653–665.

Herrmann, G., Lindahl, T., and Schar, P. (1998). Saccharomyces cerevisiae LIF1: a function involved in DNA double-strand break repair related to mammalian XRCC4. EMBO J. *17*, 4188–4198.

Kishi, H., Borgulya, P., Scott, B., Karjalainen, K., Traunecker, A., Kaufman, J., and von Boehmer, H. (1991). Surface expression of the beta T cell receptor (TCR) chain in the absence of other TCR or CD3 proteins on immature T cells. EMBO J. *10(1)*, 93–100.

Kuhn, R., Rajewsky, K., and Muller, W. (1991). Generation and analysis of interleukin-4 deficient mice. Science *254*, 707–710.

Lakso, M., Pichel, J.G., Gorman, J.R., Sauer, B., Okamoto, Y., Lee, E., Alt, F.W., and Westphal, H. (1996). Efficient in vivo manipulation of mouse genomic sequences at the zygote stage. Proc. Natl. Acad. Sci. USA *93*, 5860–5865.

Li, Z., Otevrel, T., Gao, Y., Cheng, H.-L., Seed, B., Stamato, T.D., Taccioli, G.E., and Alt, F.W. (1995). The XRCC4 gene encodes a novel protein involved in DNA double-strand break repair and V(D)J recombination. Cell *83*, 1079–1089.

Li, G.C., Ouyang, H., Li, X., Nagasawa, H., Little, J.B., Chen, D.J., Ling, C.C., Fuks, Z., and Cordon-Cardo, C. (1998). Ku70: a candidate tumor suppressor gene for murine T cell lymphoma. Mol. Cell *2*, 1–8.

Lin, S.C., Skapek, S.X., and Lee, E.Y. (1996). Genes in the RB pathway and their knockout in mice. Semin. Cancer Biol. *7*, 279–289.

Malynn, B.A., Blackwell, T.K., Fulop, G.M., Rathbun, G.A., Furley, A.J.W., Ferrier, P., Heinke, L.B., Phillips, R.A., Yancopoulos, G.D., and Alt, F.W. (1988). The *scid* defect affects the final step of the immunoglobulin VDJ recombinase mechanism. Cell *54*, 453–460.

Manis, J., Gu, Y., Lansford, R., Sonoda, E., Ferrini, R., Davidson, L., Rajewsky, K., and Alt, F. (1998). Ku70 is required for late B cell development and immunoglobulin heavy chain class switching. J. Exp. Med. *187*, 2081–2089.

Merry, D.E., and Korsmeyer, S.J. (1997). Bcl-2 gene family in the nervous system. Annu. Rev. Neurosci. *20*, 245–267.

Mizuta, R., Chen, H.Y.G., and Alt, F.A. (1997). Molecular genetic characterization of XRCC4 function. Int. Immunol. *9*, 1607–1613.

Mombaerts, P., Iacomini, J., Johnson, R.S., Herrup, K., and Tonegawa, S. (1992). RAG-1-deficient mice have no mature B and T lymphocytes. Cell *68*, 869–877.

Motoyama, N., Wang, F., Roth, K.A., Sawa, H., Nakayama, K.-I., Nakayama, K., Negishi, I., Senju, S., Zhang, Q., Fuji, S., and Loh, D.Y. (1995). Massive cell death of immature hematopoietic cells and neurons in Bcl-x-deficient mice. Science *267*, 1506–1510.

Nornes, H.O., and Carry, M. (1978). Neurogenesis in spinal cord of mouse: an autoradiographic analysis. Brain Res. *159*, 1–6.

Nussenzweig, A., Chen, C., da Costa Soares, V., Sanchez, M., Sokol, K., Nussenzweig, M.C., and Li, G.C. (1996). Requirement for Ku80 in growth and immunoglobulin V(D)J recombination. Nature *382*, 551–555.

Ouyang, H., Nussenzweig, A., Kurimasa, A., Soares, V.C., Li, X., Cordon-Cardo, C., Li, W., Cheong, N., Nussenzweig, M., Iliakis, G., Chen, D.J., and Li, G.C. (1997). Ku70 is required for DNA repair but not for T cell antigen receptor gene recombination in vivo. J. Exp. Med. *186*, 921–929.

Schar, P., Herrmann, G., Daly, G., and Lindahl, T. (1997). A newly identified DNA ligase of Saccharomyces cerevisiae involved in RAD52-independent repair of DNA double-strand breaks. Genes Dev. *11*, 1912–1924.

Shinkai, Y., Rathbun, G., Lam, K., Oltz, E., Stewart, V., Mendelsohn, M., Charon, J., Datta, M., Young, F., Stall, A., and Alt, F. (1992). RAG-2 deficient mice lack mature lymphocytes due to an inability to initiate V(D)J recombination. Cell *68*, 855–867.

Shortman, K., Egerton, M., Spangrude, G.J., and Scollay, R. (1990). The generation and fate of thymocytes. Semin. Immunol. *2*, 3–12.

Smider, V., and Chu, G. (1997). The end-joining reaction in V(D)J recombination. Sem. Immunol. *9*, 189–197.

Stamato, T.D., Weinstein, R., Giaccia, A., and Mackenzie, L. (1983). Isolation of cell cycle-dependent gamma-ray-sensitive Chinese hamster ovary cell. Somat. Cell Genet. *9*, 165–173.

Stamato, T., Guerriero, S., and Denko, N. (1993). Two methods for assaying DNA double-strand break repair in mammalian cells by asymmetric field inversion gel electrophoresis. Radiat. Res. *133*, 60–66.

Taccioli, G., Amatucci, A., Beamish, H., Gell, D., Xiang, X., Arzayus, M., Priestley, A., Jackson, S., Rothstein, A., Jeggo, P., and Herrera, V. (1998). Targeted disruption of the catalytic subunit of the DNA-PK gene in mice confers severe combined immunodeficiency and radiosensitivity. Immunity *9*, 355–366.

Teo, S.-H., and Jackson, S.P. (1997). Identification of Saccharomyces cerevisiae DNA ligase IV: involvement in DNA double-strand break repair. EMBO J. *16*, 4788–4795.

Tourigny, M.R., Mazel, S., Burtrum, D.B., and Petrie, H.T. (1997). T cell receptor (TCR)-beta gene recombination: dissociation from cell cycle regulation and developmental progression during T cell ontogeny. J. Exp. Med. *185*, 1549–1556.

Wilson, T.E., Grawunder, U., and Lieber, M.R. (1997). Yeast DNA ligase IV mediates non-homologous DNA end joining. Nature *388*, 495–498.

Wuerffel, R.A., Du, J., Thompson, R.J., and Kenter, A.L. (1997). Ig $S\gamma 3$ DNA-specifc double strand breaks are induced in mitogen-activated B cells and are implicated in switch recombination. J. Immunol. *159*, 4139–4144.

Zhu, C., Bogue, M.A., Lim, D.-S., Hasty, P., and Roth, D.B. (1996). Ku86-deficient mice exhibit severe combined immunodeficiency and defective processing of V(D)J recombination intermediates. Cell *86*, 379–389.